ANTIOXIDANTS & REDOX SIGNALING
Volume 13, Number 1, 2010

DOI: 10.1089/ars.2009.2886

ORIGINAL RESEARCH COMMUNICATION

PAMM: A Redox Regulatory Protein That Modulates Osteoclast Differentiation

Yan Xu,[1,*,†] Leslie R. Morse,[2,†] Raquel Assed Bezerra da Silva,[3] Paul R. Odgren,[4] Hajime Sasaki,[1] Philip Stashenko,[1] and Ricardo A. Battaglino[1]

Abstract

The central role of reactive oxygen species (ROS) in osteoclast differentiation and in bone homeostasis prompted us to characterize the redox regulatory system of osteoclasts. In this report, we describe the expression and functional characterization of PAMM, a CXXC motif–containing peroxiredoxin 2–like protein expressed in bone marrow monocytes on stimulation with M-CSF and RANKL. Expression of wild-type (but not C to G mutants of the CXXC domain) PAMM in HEK293 cells results in an increased GSH/GSSG ratio, indicating a shift toward a more reduced environment. Expression of PAMM in RAW264.7 monocytes protected cells from hydrogen peroxide–induced oxidative stress, indicating that PAMM regulates cellular redox status. RANKL stimulation of RAW 264.7 cells caused a decrease in the GSH/GSSG ratio (reflecting a complementary increase in ROS). In addition, RANKL-induced osteoclast formation requires phosphorylation and translocation of NF-κB and c-Jun. In stably transfected RAW 264.7 cells, PAMM overexpression prevented the reduction of GSH/GSSG induced by RANKL. Concurrently, PAMM expression completely abolished RANKL-induced p100 NF-κB and c-Jun activation, as well as osteoclast formation. We conclude that PAMM is a redox regulatory protein that modulates osteoclast differentiation *in vitro*. PAMM expression may affect bone resorption *in vivo* and help to maintain bone mass. *Antioxid. Redox Signal.* 13, 27–37.

Introduction

Reactive oxygen species (ROS) and other intracellular free radicals are involved in the control of many cellular functions, including proliferation, activation, growth inhibition, regulation of the activity of transcription factors (14, 17), and apoptosis (16). Yet, at high concentrations, ROS can cause oxidative stress and induce harmful events like inflammatory response, apoptosis, or ischemia (13). Cells have developed several redox systems to protect themselves against cytotoxic effects of ROS. Oxidative stress, which results in changes in the redox status of cells, plays important roles in aging as well as in many diseases, including malignancies, diabetes, neurodegenerative diseases, atherosclerosis, ischemia, autoimmunity, and HIV infection (14, 15)

Free radicals also are involved in the pathogenesis of osteoporosis (6). Dietary antioxidants (18, 25), levels of plasma antioxidants (5, 24), and oxidative stress (4) have been all linked with bone density and the risk of hip fracture. At the cellular level, ROS have been found to stimulate osteoclastic bone resorption (22, 23) and osteoclast differentiation (3, 9), whereas free radical scavengers and antioxidants are inhibitory. ROS, conversely, inhibit osteoblast differentiation (2) and cause osteocyte apoptosis (20). Bone remodeling is regulated by the concerted action of osteoblasts (bone formation) and osteoclasts (bone resorption). Imbalances in the activity or number of osteoblasts and osteoclasts (or both) can lead to increases or decreases in bone resorption. This results in several skeletal diseases, such as osteoporosis, metastatic bone disease and Paget disease (characterized by increased bone resorption) or various types of osteopetrosis (characterized by decreased bone resorption).

Redox status affects bone metabolism, including osteoclast differentiation (18). Thiol antioxidants are mediators of estrogen deficiency–induced bone loss. In one study, researchers found decreased levels of glutathione, glutathione

[1]Department of Cytokine Biology, The Forsyth Institute, and the [2]Department of Physical Medicine and Rehabilitation, Harvard University School of Medicine, Boston, Massachusetts.
[3]Department of Pediatric Clinic, Preventive and Community Dentistry, School of Dentistry of Ribeirão Preto, University of São Paulo, São Paulo, Brazil.
[4]Department of Cell Biology, University of Massachusetts Medical School, Worcester, Massachusetts.
*Current affiliation: Kunming Medical University, China.
†These authors contributed equally to this work.

reductase, thioredoxin-1 (Trx-1), and Trx reductase in bone marrow (but not liver or spleen) after ovariectomy. Furthermore, this response was rapidly reversed by treatment with 17-β estradiol and was prevented by antioxidants. Finally, buthionine-(*S*,*R*)-sulfoxime (BSO), an inhibitor of glutathione synthesis, caused bone loss. Bone resorption after estrogen deficiency might be attributed, in part, to reduced antioxidant defenses in osteoclasts or other cells or both in the bone marrow (22). Osteoclast differentiation and function was shown to be regulated by cellular redox status in a biphasic way (21), and cellular redox status has been shown to modulate the nuclear import of transcription factors (1, 18). Furthermore, collectively, these results demonstrate that cellular redox status affects bone remodeling, at least in part by regulating osteoclast differentiation.

Two related families of proteins, peroxiredoxins (PRXs) and thioredoxins (TRXs), are important regulators of cellular redox status in bone and other tissues. PRXs confer a protective antioxidant role in cells through their peroxidase activity, in which hydrogen peroxide, peroxynitrate, and organic hydroperoxides are reduced and detoxified. TRXs, conversely, alter the redox state of target proteins by catalyzing the reduction of their disulfide bonds through a CXXC motif by using reducing equivalents derived from either NADPH or ferredoxins.

In this report, we describe a new member of the peroxiredoxin (PRX)-like 2 family, which we have named *PAMM* (peroxiredoxin (PRX)-like 2 activated in M-CSF stimulated monocytes). Members of this family show sequence similarity to peroxiredoxins. In addition, (PRX)-like 2 proteins, like PAMM, are similar to thioredoxin in that they contain a CXXC motif, used by many enzymes with redox regulatory functions. We demonstrate that PAMM is expressed in bone, brain, liver, and kidney and also is found in bone marrow monocytes on stimulation with M-CSF and RANKL. We characterize PAMM expression and activity as well as its role during osteoclast differentiation. We propose in this report that RANKL-induced osteoclast differentiation requires PAMM downregulation and a consequent increase in ROS.

Materials and Methods

Microarray hybridization

A genome-wide expression screening was conducted to identify genes upregulated during RANKL-induced osteoclast differentiation, as described previously (7). In brief, total RNA was extracted from: undifferentiated RAW 264.7 monocytes, osteoclasts derived from RAW 264.7 cells stimulated for 4 days with RANKL, undifferentiated mouse bone marrow cells (BMMs), and BMMs stimulated with M-CSF + RANKL for 7 days. The RNA was used as a template to generate mixed cDNA probes by reverse transcription. These probes were hybridized to the Mouse MG-U74Av2 chip from Affymetrix, according to the manufacturer's instructions, at the Harvard Bauer Center for Genomics Research (Cambridge, MA).

Reagents

Antibodies against β-actin (no. 4967), NF-κB2 p100/p52 (no. 4882), Phospho-NF-κB2 p100 (Ser866/870) (no. 4810), Phospho-c-Jun (Ser243) (no. 2994), and Phospho-c-Jun (Ser 63) (no. 9261) were purchased from Cell Signaling Technology, Inc. (Danvers, MA). Anti-C10orf58 (PAMM) antibody (HPA009025) was purchased from Sigma (St. Louis, MO). G418 was purchased from Invitrogen (Carlsbad, CA).

Cell culture

RAW 264.7 mouse monocytes (TIB-71) were purchased from ATCC (Manassas, VA). Cells were cultured in DMEM with 1.5 g/L sodium bicarbonate plus 10% non–heat-inactivated FBS (Invitrogen). DMEM was supplemented with 50 ng/ml recombinant mouse soluble RANKL (PeproTech, Inc., Rocky Hill, NJ) for 4 days. Human peripheral blood mononuclear cells (PBMCs) were isolated from PBS-diluted blood (1:1, vol/vol) by centrifugation on a Histopaque-1077 (Sigma) density gradient. $CD14^+$ selection was performed by using the Human CD14 Selection Cocktail (StemCell Technologies, catalog no. 18058). $CD14^+$ PBMCs were cultured for 4 days in α-MEM/10% FBS supplemented with 180 ng/ml human RANKL (PeproTech Inc., Rocky Hill, NJ) and 150 ng/ml human M-CSF (PeproTech Inc.). HEK 293 cells were maintained in DMEM/10% FBS.

Animals

Animals were obtained from the breeding colony of toothless (*tl*) rats maintained at the University of Massachusetts Medical School, and all procedures involving animals were approved by the UMMS IACUC. t*l* is an autosomal, dominant, null mutation the *Csf-1* gene (31). CSF-1–induced gene-expression changes in *tl*/*tl* rats during the time course of CSF-1 injections was described in detail in Yang *et al.* (32). In brief, animals were injected IP daily with 10^6 units of recombinant human M-CSF (Chiron) for 4 days. One tibia was fixed in *p*-formaldehyde and prepared for histologic analysis.

Quantitative RT-PCR and Western blot

Total RNA was extracted from cells and tissues by using the TRIAZOL reagent (Invitrogen), following the manufacturer's instructions. For RT-PCR, 2 μg of RNA was reverse-transcribed into cDNA by using SuperScript II (Invitrogen, no. 18064-022) by following the manufacturer's instructions. Real-time reverse transcription–polymerase chain reaction (RT-PCR) was conducted by using the DyNAmo SYBR Green qPCR Kit (Finnzymes, Espoo, Finland) in a 24-μl reaction volume containing 1 μl of a 1:4 dilution of first-strand reaction product, 1 μl of 10 μM gene-specific upstream and downstream primers mixture. Amplification and analysis of cDNA fragments were carried out by using a 7300 real-time PCR system (ABI, Foster City, CA). Cycling conditions were initial denaturation at 95°C for 10 min, followed by 40 cycles consisting of a 15-s denaturation interval at 95°C, and a 1-min annealing and extension interval at 60°C. Amplification of human β-actin mRNA, the housekeeping gene, was used as an endogenous control to normalize results. Levels of mRNA expression were measured as threshold levels (Ct) and normalized with the individual β-actin control Ct values. The primer sequences were as follows: human *pamm* (C10orf58) sense, 5′-ATA GAC CTG AAA ACA CTG GA-3′, and antisense, 5′-GCA GCT TCC TCT CGA CAG AG-3′; human β-actin, sense, 5′-CTC TTC CAG CCT TCC TTC CT-3′, and antisense, 5′-AGC ACT GTG TTG GCG TAC AG-3′.

Protein lysates were generated by resuspending cells in Novex Tris-Glycine SDS Sample Buffer (2x) (Invitrogen).

Equivalent amounts of protein were loaded onto Novex Tris-Glycine SDS gels (Invitrogen), electrophoresed, and transferred to nylon membranes by following the manufacturer's instructions. After blocking, membranes were incubated with the indicated primary antibodies overnight at 4°C, washed to remove unbound antibody, and incubated with secondary antibody for 1 h at room temperature. Chemiluminescent signal was detected by using the LUMIGLO reagents A and B (Cell Signaling Technology (Danvers, MA; no. 7003) by following the manufacturer's instructions. Blots were then exposed to x-ray film.

Immunohistochemistry

Antigen detection on deparaffinized bone sections was performed according to standard protocols. In brief, sections were incubated in a humidified chamber overnight at 4°C in primary antibody at the indicated dilutions. The following day, the slides were washed 3×10 min in 1×PBS + 0.1% (vol/vol) Tween-20. Sections were then incubated for 1 h at room temperature with the biotinylated secondary antibody (100 μl/section, diluted 1:250 to 1:750 in blocking buffer) in a humidified chamber. Finally, slides were washed 3×10 in 1× PBS and incubated with one drop of ABC (Ready-to-use Vectastain ABC Kit, Vector Laboratories, Inc., Burlingame, CA), incubated for 30 min at room temperature, washed 3×5 min in 1× PBS, and incubated for 2 to 10 min with DAB solution until signal developed. Images were acquired with a LEICA DMLS optical microscope equipped with a LEICA DC 100 digital imaging system.

Fluorescent photomicrographs were taken with an OLYMPUS BX51TRF microscope. Images were captured with CytoVision version 3.93 Software.

Plasmids, generation of mutants, transfections

An expression plasmid (SC105291) was purchased from OriGene Technologies (Rockville, MD). This plasmid contains the entire cDNA for human *pamm*. Site-directed mutagenesis was performed by using the Phusion® Site-Directed Mutagenesis Kit (New England Biolabs F-541S) by following the manufacturer's instructions. The following primers were used to generate the ^{85}CXX^{88}C mutants

^{85}C to G:
Sense: (DNA)-Phos-GGT TTC CTC TGT CGA GAG GAA GCT
Antisense: (DNA)-Phos-GCC TGG CCT CCG CAC GGC CAT AAT
^{88}C to G:
Sense: (DNA)-Phos-GGT CGA GAG GAA GCT GCG GAT CTG
Antisense: (DNA)-Phos-GAG GAA ACA GCC TGG CCT CCG CAC

RAW 264.7 and HEK 293 cells were transfected with the indicated plasmids by using the Lipofectamine 2000 Transfection Reagent (Invitrogen, no. 11668-019) by following the manufacturer's instructions. For the generation of stable transfectants, we made pIRESneo3/PAMM, in which we inserted a NotI-1,000-bp fragment from SC105291 into pIRESneo3 (Clontech Laboratories, Inc., Mountain View, CA). The NotI insert contains the entire ORF plus 5′ UTR and 3′ UTR. The vector contains the internal ribosome entry site (IRES) of the encephalomyocarditis virus, which permits the translation of two open reading frames (*pamm* and neomycin phosphotransferase) from one messenger RNA. Transfected cells were selected with G418, and nearly all surviving colonies stably expressed PAMM. The expression cassette of pIRESneo3 contains the human CMV major immediate early promoter.

Measurement of GSH/GSSG ratio

RAW264.7 cells were cultured with RANKL to induce osteoclast differentiation, harvested at 1-day intervals for 4 days, and stored at −70°C until use. The GSH/GSSG ratio was measured with the glutathione reductase/5,5′-dithiobis-(2-nitrobenzoic acid) (DTNB) assay kit (Bioxytech GSH-412, OXIS International, Beverly Hills, CA) according to the manufacturer's instructions. In brief, total glutathione (GSH_t) and GSSG concentrations were derived from GSH and GSSG standard curves and converted to nanomoles per milligram of protein. Reduced GSH concentrations were found by subtracting GSSG from total glutathione. Finally, the GSH/GSSG ratio was calculated by dividing the difference between total glutathione and GSSG concentrations by the GSSG concentration [ratio = GSHt – 2 (GSSG)/GSSG].

Cell-viability assay

Cells were plated at a density of 10^4 cells/well on 96-well plates in 100 μl DMEM. Cell viability was evaluated by using the MTT Based Cell Growth Determination Kit (Sigma-Aldrich, Cat. no. CGD-1) by following the manufacturer's instructions. The amount of MTT formazan produced (which is proportional to cell number) was determined by measuring absorbance with a microplate reader (Bio-Rad, Hercules, CA) at a test wavelength of 570 nm and a reference wavelength of 630 nm.

H_2O_2 treatment

H_2O_2 was diluted in PBS and further diluted in culture medium to the indicated concentrations. Cells were incubated in H_2O_2-containing medium for 24 h.

Statistical analysis

Data are presented as means plus or minus 1 SD from at least three independent experiments. Statistical significance was determined by using one-way analysis of variance (ANOVA) followed by the Student *t* test (*$p < 0.05$; **$p < 0.005$).

Results

Identification of pamm: sequence, structure, and orthologues

We previously performed a genome-wide microarray screening in RAW 264.7 cells as well as in normal BMM stimulated with RANKL and with M-CSF + RANKL, respectively (7) to identify genes involved in RANKL-induced osteoclast formation. Unstimulated cells were used as controls. We selected only genes whose expression was upregulated in both cellular model systems of osteoclast differentiation (RAW 264.7 and BMM). A summary of the results is shown in

Table 1. Summary of Results of Affymetrix Screening

Affymetrix probe set[a]	*Gene name*	p *Value (RAW)*	p *Value (BMM)*
98859_at	Acid phosphatase 5, tartrate-resistant Acp5, *trap*	0	0
160901_at	*c-fos*	0	0
160406_at	*Cathepsin K*	0	0
99957_at>	*mmp-9*	0	0
104388_at C	*mip-1γ*	0	0
96481_at	NHAoc/NHA2	0.000001	0
96634_at	*pamm*, C10orf58	0.000004	0.000009
Cell system[b]	*Fold change (unstimulated* vs. *stimulated)*		
BMM	1.483		
RAW 264.7	1.415		

[a]A partial list displays the top-ranking genes identified in the screening.
[b]Induction of PAMM in bone marrow monocytes and RAW 264.7 cells.

Table 1A. The *p* value calculated for each gene indicates the probability of a RANKL-induced increase in gene expression, with a *p* value near or equal to zero indicating very high likelihood. Some of the top genes identified in this screening are well-known osteoclast-specific genes—*trap*, *c-fos*, *cathepsin K*, *mmp-9*—which validate our screening protocol. We also detected *mip-1γ*, which we found to mediate RANKL-induced osteoclast formation and survival (27), and NHAoc/NHA2, a novel gene whose expression is restricted to osteoclasts and is required for osteoclast terminal differentiation (8, 28).

We identified another gene, which we named *pamm* [Peroxiredoxin (PRX)-like 2 Activated in M-CSF stimulated monocytes]. *pamm* mRNA is upregulated in stimulated RAW 264.7 cells and BMM (fold changes relative to unstimulated cells: 1.41 and 1.48, respectively; Table 1B). *pamm* is a member of the peroxiredoxin (PRX)-like 2 family, which is identical to an uncharacterized human gene: *Homo sapiens* chromosome 10 open reading frame 58 or C10orf58 (NCBI Reference Sequence: NM_032333.4). Orthologues of *pamm* are present throughout the animal kingdom, including invertebrates (see http://www.ncbi.nlm.nih.gov/Structure/cdd/cddsrv.cgi?uid=48519 for additional information and sequence alignment data). *pamm* nucleotide-sequence analysis predicts the existence of a 229-amino acid protein: PAMM (Fig. 1). Members of this family of proteins show sequence similarity to peroxiredoxins (PRXs). In addition, they contain a CXXC motif, similar to that of thioredoxins (TRXs). The CXXC motif is used to alter the redox state of target proteins by catalyzing the reduction of their disulfide bonds. PAMM contains a putative CXXC motif (C in positions 85 and 88), which suggests that PAMM has redox activity.

PAMM is expressed in M-CSF–activated macrophages in vitro *and* in vivo

Western blot analysis of multiple mouse tissues revealed that PAMM is expressed in kidney, liver, skin, and brain (Fig. 2A). PAMM also is found in $CD14^+$ human peripheral blood mononuclear cells (PBMCs) on stimulation with M-CSF and RANKL (Fig. 2B). Although the upregulation of PAMM detected in differentiated human PBMCs is modest, it is not the result of uneven loading, because we could not detect PAMM expression in unstimulated PBMCs, even when the blots were exposed for long periods (20 min; data not shown). Moreover, this level of PAMM upregulation is in agreement with the expression fold change (1.48) obtained for *pamm* RNA (Fig. 1B). To study *pamm* expression further during macrophage activation and osteoclast differentiation, we cultured $CD14^+$ human PBMCs in the presence of M-CSF alone or M-CSF and RANKL, obtained total RNA from these cells, and determined *pamm* relative quantification (RQ) with quantitative RT-PCR. RQ is commonly used to determine gene-expression levels in different samples (for instance, undifferentiated vs. differentiated cells). The target molecule value is normalized with a reference gene (in our case, *β*-actin). Quantitative RT-PCR analysis confirms that although no *pamm* mRNA is expressed in unstimulated $CD14^+$ PBMCs, expression increases (approximately sevenfold) in M-CSF–

```
        10          20          30          40          50          60
MSFLQDPSFF  TMGMWSIGAG  ALGAAALALL  LANTDVFLSK  PQKAALEYLE DIDLKTLEKE

        70          80          90         100         110         120
PRTFKAKELW  EKNGAVIMAV  RRPGCFLCRE  EAADLSSLKS  MLDQLGVPLY  AVVKEHIRTE
                        *  *
       130         140         150         160         170         180
VKDFQPYFKG  EIFLDEKKKF  YGPQRRKMMF  MGFIRLGVWY  NFFRAWNGGF  SGNLEGEGFI

       190         200         210         220
LGGVFVVGSG  KQGILLEHRE  KEFGDKVNLL  SVLEAAKMIK  PQTLASEKK
```

FIG. 1. Amino acid sequence of human PAMM. PAMM nucleotide sequence contains an open reading frame that codes for a 229–amino acid protein. The amino acid sequence predicts a cytoplasmic protein. The asterisks indicate C85 and C88, flanking the CXXC motif.

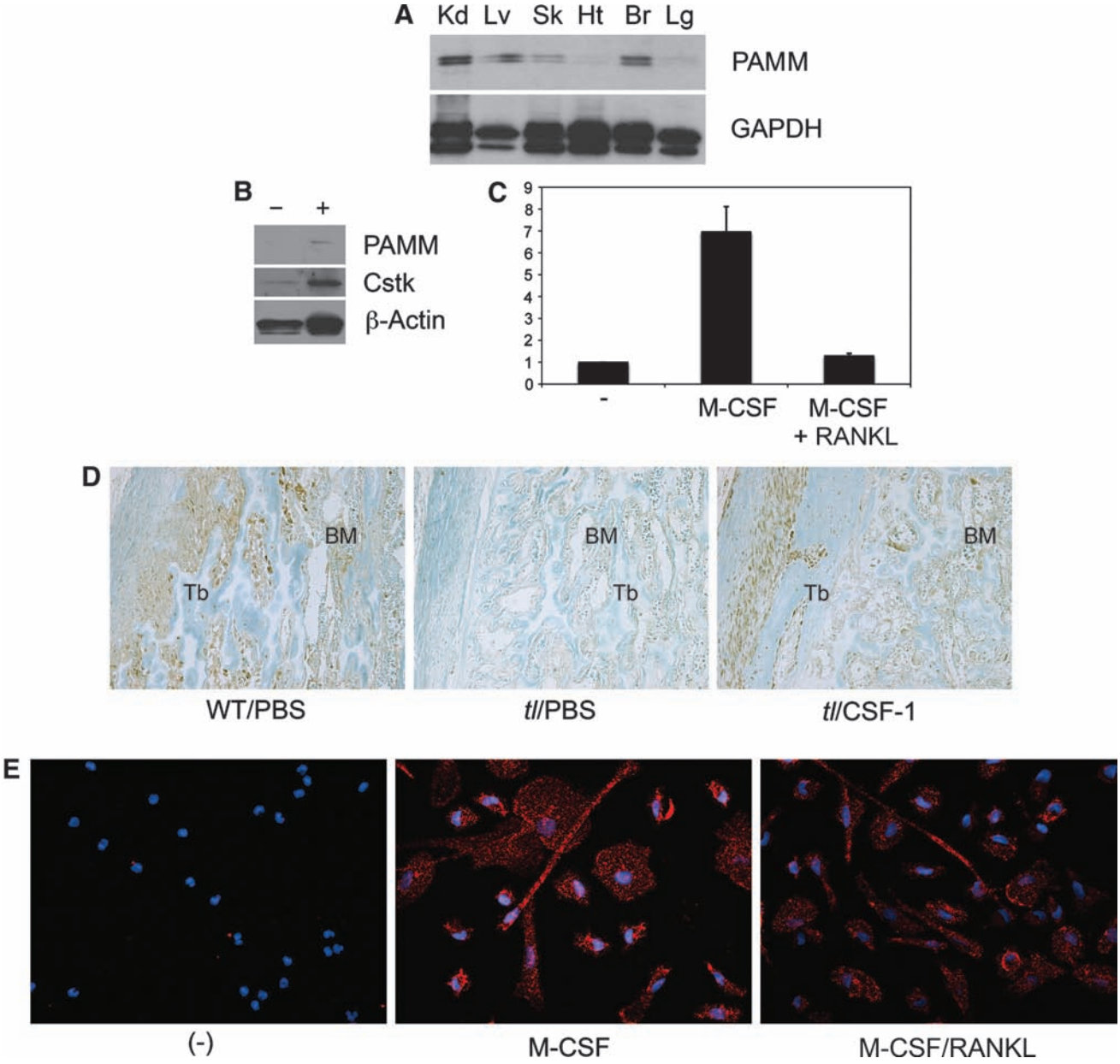

FIG. 2. PAMM expression: mRNA and protein studies. (**A**) Western blot analysis of mouse proteins shows expression of PAMM (a band of ~25 kDa) in multiple tissues. Kd = kidney; Lv = liver; Sk = skin; Ht = heart; Br = brain; Lg = lung. (**B**) Western blot analysis of PAMM of protein from human PBMCs shows expression of PAMM under different conditions: (−) unstimulated, and (+) stimulated with M-CSF plus RANKL. *β*-Actin was used as a control for loading, *Cathepsin k* (Cstk) was used as a control for differentiation in human PBMCs. (**C**) Relative quantification (RQ) of *pamm* compared with *β-actin*, as determined with quantitative RT-PCR analysis of mRNA from human PBMCs: (−) unstimulated; M-CSF, stimulated with M-CSF; M-CSF + RANKL, stimulated with M-CSF plus RANKL for 7 days (the results are expressed as mean ± SD; $n = 3$). (D) Histochemical analysis of tibia sections from wild-type (WT) and Toothless (tl/tl) rats by using an anti-PAMM antibody. The micrographs (magnification, 20×) show that PAMM expression in bone marrow monocytes (BMMs) is upregulated by CSF-1 treatment (compare left and center panels). Tb = trabecular bone; BM = bone marrow. (**E**) Immunocytochemical analysis of osteoclasts derived from human $CD14^+$ PBMCs stained with an anti-PAMM antibody and a secondary antibody conjugated to Alexa Fluor 594. Cells were also stained with DAPI, a nuclear fluorescent dye. The micrographs (magnification, 20×) of unstimulated cells (*left*) show only DAPI (blue) staining. M-CSF–stimulated cells (*center*) show DAPI staining and a strong cytoplasmic PAMM signal (red). PAMM signal decreases in cells stimulated with M-CSF plus RANKL (*right panel*).

stimulated cells (Fig. 2C). Stimulation with both M-CSF and RANKL, conversely, resulted in a reduction of *pamm* mRNA (Fig. 2C).

Finally, we investigated the expression of PAMM in bone marrow monocyte activation *in vivo,* induced by M-CSF in bone sections from *Csf-1*-null toothless (*tl/tl*) rats (32). PAMM increased significantly in bone marrow cells in *tl* rats treated with M-CSF for 4 days (Fig. 2D) compared with that in untreated controls. Levels of expression were comparable to those observed in wild-type rats. These results confirm that

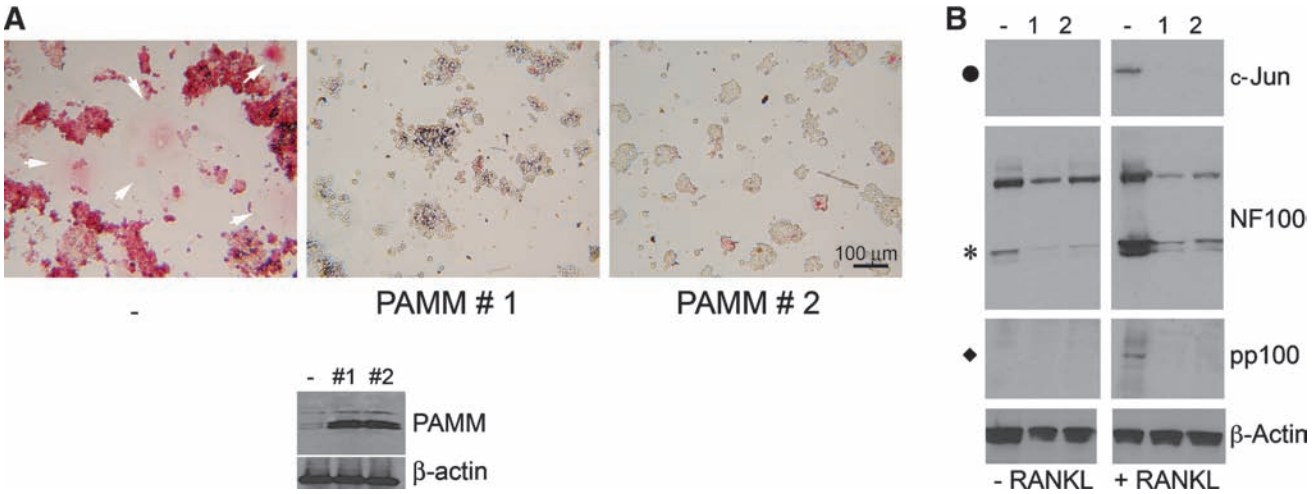

FIG. 3. PAMM expression blocks RANKL-induced NF-κB2 and c-Jun activation as well as osteoclast differentiation. Two stably transfected clones of PAMM-expressing RAW 264.7 cells (PAMM 1 and 2) were incubated for 5 days on plastic coverslips in the presence of RANKL (100 ng/ml). Cells stably transfected with an empty vector were used as controls. (**A**, *top panel*) *TRAP* staining (red) of control RAW 264.7 cells (-) stimulated for 5 days with RANKL show abundant positive cells as well as many giant multinucleated osteoclasts (*white arrowheads*). *TRAP*-stained cells derived from stimulation of PAMM 1 (1) and 2 (2) (two independent RAW 264.7 clones stably transfected with a PAMM expression vector) show virtually no positive cells. (**A**, *bottom panel*) Western blot analysis of protein extracts from control RAW264.7, PAMM 1, and PAMM 2 cells by using an anti-PAMM and β-actin antibody shows that PAMM 1 and PAMM 2 cells overexpress PAMM. (**B**) Western blot analysis of protein samples from cells stimulated with RANKL for 24 h indicate phosphorylation/activation of c-Jun (*top right panel*, indicated by ●) in control cells (−). No activation can be seen in either PAMM 1 or 2 cells (1, 2). Similar results can be observed for NF-κB2 p100/p52 cleavage (*center right*, indicated by *) and NF-κB2 p100 phosphorylation in Ser866/870) (*bottom right*, indicated by ◆).

M-CSF stimulation can activate PAMM expression in BMM *in vivo*. Finally, immunocytochemical analysis of human PBMCs incubated with a specific anti-PAMM antibody (Fig. 2E) confirms that M-CSF alone, as well as M-CSF/RANKL, can stimulate expression of PAMM, but expression is higher in M-CSF–stimulated cells.

Overexpression of PAMM inhibits NF-κB and c-Jun activation and OC differentiation

Our observation that stimulation with RANKL resulted in decreased PAMM expression in M-CSF–stimulated monocytes (Fig. 2C and E) suggested that downregulation of PAMM is required for RANKL-induced osteoclast formation. RANKL-induced osteoclast formation and activation requires the activation of the transcription factors NF-κB2 and AP-1 (3, 18). NF-κB2 activation, in turn, is augmented by ROS (18). To study the possible effect of PAMM expression on ROS production and osteoclast differentiation, we generated stable RAW264.7 cell lines constitutively expressing PAMM and compared the ability of RANKL to induce NF-κB2 and c-Jun activation, as well as osteoclast differentiation in two independent stably-transfected cell lines (PAMM 1 and 2) *versus* control (stably transfected with an empty vector) cells. We found that constitutive expression of PAMM virtually abolished osteoclast formation, as judged by the formation of osteoclast-like *TRAP*-positive multinuclear cells (Fig. 3A, PAMM 1 and PAMM 2). Western blot analysis of protein extracts from those cells (Fig. 3A, bottom panel) confirmed that cell lines PAMM 1 and PAMM 2 overexpress PAMM. In a parallel series of experiments, we incubated RAW264.7 cells stably transfected with either PAMM or empty vector with 50 ng RANKL for 24 h and prepared protein extracts to analyze them for activation of NF-κB2 (as shown by cleavage and phosphorylation of NF100) and c-Jun. We found that, whereas NF-κB2 and c-Jun were strongly activated in control RAW264.7 cells (Fig. 3B, lane −), activation was essentially abolished in PAMM-RAW264.7 cells (Fig. 3B, lanes 1 and 2), suggesting that PAMM overexpression blocks RANKL induced osteoclast differentiation by inhibiting NF-κB2 and c-Jun activation.

PAMM expression increases cellular GSH/GSSG ratio and protects cells from oxidative stress

During osteoclast differentiation, the GSH/GSSG ratio, a proxy for cellular redox status, decreases in response to M-CSF and RANKL stimulation. Differentiation of RAW 264.7 monocytes as well as bone marrow monocytes (BMMs) was associated with a time-dependent decrease in the GSH/GSSG ratio and a corresponding increase of ROS (18). To examine whether expression of PAMM could affect the decrease of GSH/GSSG ratio that follows RANKL stimulation, we stimulated RAW 264.7 PAMM 1 cells with RANKL for 4 days and determined the GSH/GSSG ratio each day. RAW264.7 cells transfected with an empty vector were used as controls. We observed a time-dependent decrease in GSH/GSSG in RAW 264.7 monocytes in response to RANKL stimulation (Fig. 4A, top), in agreement with previous reports (18). In PAMM-expressing cells, conversely, the GSH/GSSG ratio increased with time (Fig. 4A, bottom). This indicates a shift toward a more-reduced cellular environment in PAMM-expressing cells, indicating that PAMM has redox regulatory activity. We also tested this hypothesis in HEK293 cells. For this, we

transiently transfected HEK293 cells with a PAMM expression plasmid, cultured transfected cells for 24 and 72 h, measured the GSH/GSSG ratio, and calculated the change in GSH/GSSG from day 1 to day 3 (Fig. 4B). In control cells (transfected with an empty vector), the Day3/Day1 ratio was 83%, a decrease that indicates a shift toward a more-oxidized environment. In PAMM-transfected cells, conversely, the Day3/Day1 change was 459%, indicating that PAMM expression shifts the redox status of the cells toward a more-reduced environment.

We also transfected cells with C85G and C88G mutants, in which cysteine residues were substituted by glycine at positions 85 and 88, respectively. These two cysteine residues form part of the CXXC domain, and presumably are essential for the ability of PAMM to regulate cellular redox status. The results (Fig. 4B) show that in cells transfected with either C85G or C88G mutants, the Day3/Day ratio decreases to 123% and 38%, respectively. These values are similar to those obtained with the empty vector, confirming that both C

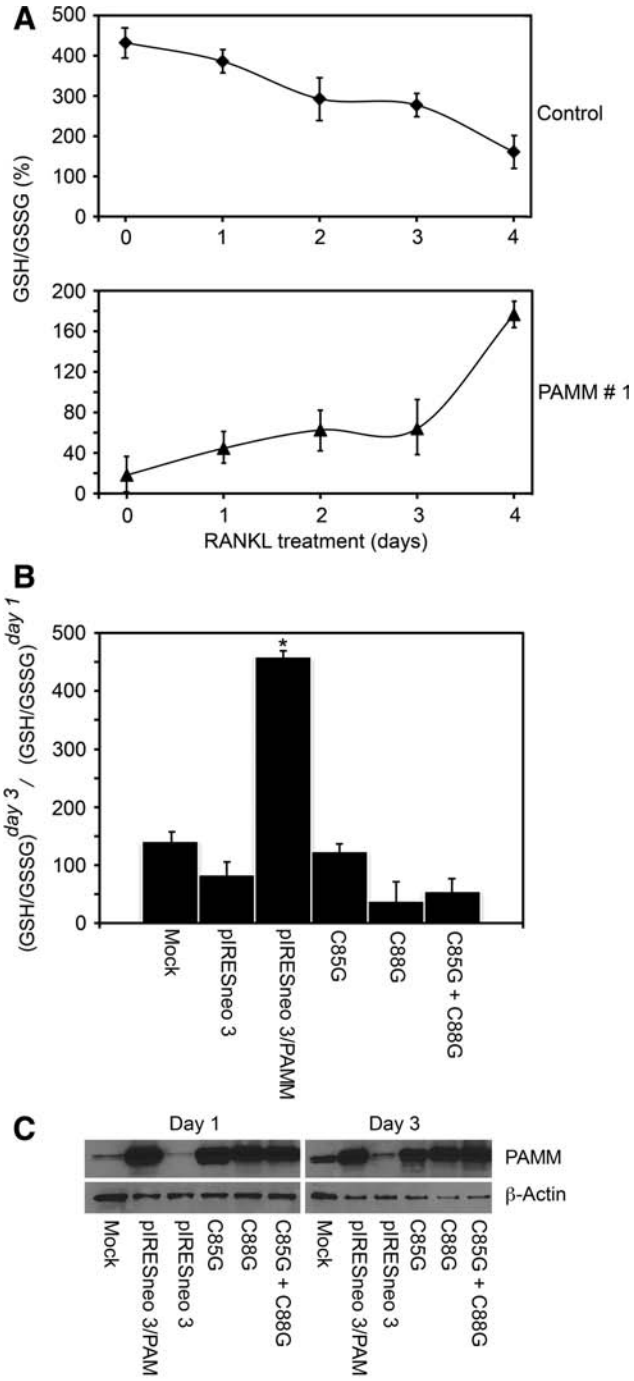

FIG. 4. PAMM expression increases the GSG/GSSG ratio. (**A**) Cells (PAMM-expressing RAW 264.7 clone 1, and RAW 264.7 control) were cultured under differentiation conditions and collected at 1-day intervals for 4 days after RANKL-induced OC differentiation. The GSH/GSSG ratio was measured in these cells' cytosolic fractions. (*Top*) GSG/GSSG ratio decreases in control RAW 264.7 cells as a result of RANKL-induced osteoclast differentiation (Control)z. (*Bottom*) GSG/GSSG ratio, conversely, increases in PAMM-expressing cells under the same conditions of stimulation, as a result of the antioxidant activity of PAMM (PAMM 1). Results are expressed as mean ± SD ($n = 3$). (**B**) HEK 293 cells were transiently transfected with a wild-type PAMM expression vector (pIRESneo3/PAMM), a mutant version of PAMM harboring a cysteine 85-to-glycine substitution (C85G), a mutant version of PAMM with a cysteine 88-to-glycine substitution (C88G), or co-transfected with C85G and C88G. Control cells were transfected with an empty vector (pIRESneo3) or mock-transfected (Mock). Cells were cultured for 1 and 3 days and harvested. The GSH/GSSG ratio was measured in these cells' cytosolic fractions, and the $GSH/GSSG^{day3}$ to $GSH/GSSG^{day1}$ was calculated and expressed as a percentage. The results indicate that both cysteines are essential for PAMM antioxidant activity. Co-transfection of both single mutants does not rescue the activity, suggesting that the protein is a functional monomer ($^*p < 0.05$). (**C**) Western blot analysis of HEK 293 cells transfected with the different versions of PAMM [as described in (**B**)] by using an anti-PAMM antibody show equivalent PAMM expression levels in all transfected cells at days 1 and 3.

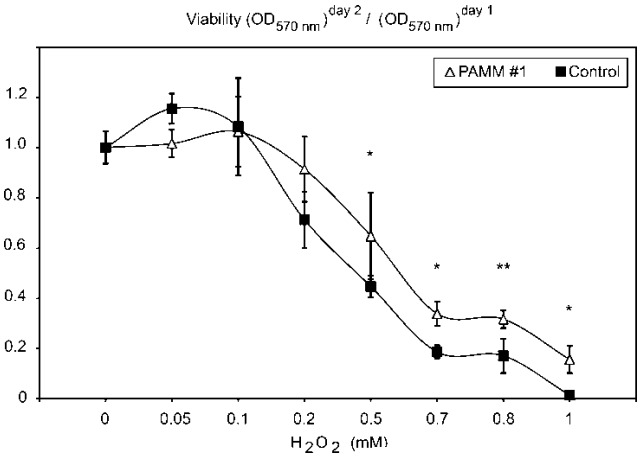

FIG. 5. PAMM expression protects cells from H_2O_2-induced oxidative stress. Cell viability decreases in a dose-dependent manner as a result of oxidative stress induced by H_2O_2 treatment of control RAW 264.7 cells (*solid black squares*). Viability is increased in PAMM 1 cells (*white triangles*) as a result of PAMM antioxidant activity. Results are expressed as mean ± SD ($n = 4$). ($^*p < 0.05$; $^{**}p < 0.005$).

residues (but ^{88}C to a larger extent) are required for PAMM activity. Finally cotransfection of both mutants (C85G and C88G) fails to rescue the antioxidant activity, which suggests that no functional complementation occurs between PAMM molecules. These values are due to differences in the activity of PAMM and not to differences in expression levels, because Western blot analysis (Fig. 4C) shows equivalent expression levels of PAMM (wild-type and mutant versions) in all transfected cells.

We next examined the ability of PAMM to protect cells from oxidative stress. For that, we cultured PAMM-stable RAW264.7 cells in the presence of H_2O_2 (ranging from 0 to 1 m*M*) for 24 h, determined cell viability with the MTT assay, and expressed it as a percentage of viability with 0 m*M* H_2O_2, as described by Tang *et al.* (30). RAW 264.7 macrophages were cultured in parallel under the same conditions. At lower concentrations (0.05 to 0.1 m*M*), H_2O_2 was not cytotoxic. At higher (0.2 to 1.0 m*M*) concentrations, however, H_2O_2 was cytotoxic in a dose-dependent manner. Compared with control cells, PAMM-RAW 264.7 cells showed a significantly greater ability to resist oxidative stress by exogenous hydrogen peroxide (Fig. 5). For instance, at 1 m*M* (a cytotoxic concentration of H_2O_2), only 1.5% of control cells retained viability, whereas more than 15% of PAMM-expressing cells were still viable. These results confirm that PAMM expression can protect cells from oxidative stress induced by H_2O_2.

The ability of PAMM to inhibit osteoclast formation depends on cysteines at positions 85 and 88

PAMM expression inhibits osteoclast differentiation in response to RANKL by increasing GSH/GSSG, with a corresponding decrease in ROS. In addition, this activity of PAMM requires cysteine residues ^{85}C and ^{88}C. If PAMM redox activity (and no other activity) is responsible for inhibition of osteoclast differentiation, then cells expressing mutants of PAMM should be able to undergo RANKL-induced osteoclast differentiation. To test this hypothesis, we transfected RAW 264.7 cells with C85G and C88G mutants as well as C85G-C88G double mutants, selected transfected cells in G418-containing media, and stimulated the transfected cells with RANKL for 4 days under differentiation conditions. As shown in Fig. 6A (top panel), both cysteine residues (^{88}C to a larger extent) are required for the ability of PAMM to inhibit RANKL-induced osteoclast differentiation, because expression of mutants C85G and C88G fail to inhibit RANKL-induced osteoclast formation to the degree that wild-type PAMM does. These results are in total agreement with the results shown in Fig. 4. That is, the more a mutation affects the redox-regulatory activity of PAMM, the more it affects its ability to inhibit osteoclast formation. Western blot analysis of protein extracts from transfected cells by using an anti-PAMM antibody confirms overexpression of PAMM in all transfected cells (Fig. 6A, bottom panel).

Finally, if PAMM inhibits osteoclast differentiation by reducing ROS cellular levels, the addition of H_2O_2 should, to a certain extent, recover the ability of PAMM-expressing cells to differentiate into osteoclasts. To test this hypothesis, we cultured PAMM-overexpressing cells (1 and 2) in the presence of RANKL plus a nontoxic concentration (50 μm) of H_2O_2. The results (Fig. 6B) clearly show that the addition of H_2O_2 rescues the ability of PAMM 1 and PAMM 2 cells to undergo RANKL-induced differentiation. Both cell lines show increased responses to the RANKL stimulus, PAMM 2 cells to a greater degree, as evidenced by formation of numerous multinucleated $TRAP^+$ cells after the addition of H_2O_2.

Discussion

We report the expression and functional characterization of a gene that we named *pamm*: peroxiredoxin (PRX)-like 2 activated in M-CSF–stimulated monocytes. This gene is identical to C10orf58, an uncharacterized gene located on human chromosome 10q23.1, which is conserved across Bilateria (http://www.ncbi.nlm.nih.gov/nucleotide/148596958). *pamm* mRNA has a 690-nucleotide open reading frame that codes for a 229-amino acid protein predicted to have cytoplasmic localization: PAMM. By immunocytochemical analysis, we showed that PAMM actually localizes to the cytoplasm. PAMM expression is enhanced in bone marrow monocytes stimulated with M-CSF and M-CSF/RANKL compared with nonstimulated macrophages, and this effect was confirmed *in vivo* by injecting M-CSF into M-CSF–negative *tl/tl* rats. Stable expression of wild-type PAMM into osteoclast precursor RAW 264.7 monocytes results in increased levels of reduced GSH and inhibits RANKL-induced osteoclastic differentiation. Expression of PAMM mutants (C85G, C88G, or C85G to C88G) in RAW 264.7 monocytes does not prevent cells from undergoing RANKL-induced osteoclast formation. Expression of the same mutants in HEK 293 cells shows that both C residues are required for PAMM redox-regulating activity. This indicates that precisely this activity of PAMM is responsible for the inhibition of osteoclast formation. Inhibition of osteoclast formation by PAMM also was associated with suppression of NF-κB2 and Jun activation.

Finally, PAMM expression protects cells against oxidative stress induced by H_2O_2 treatment. Taken together, these data shows that PAMM has redox-regulatory activity.

FIG. 6. Mutations in the CXXC motif and the addition of H_2O_2 abolish PAMM ability to inhibit osteoclast formation. (**A**, *top panel*) Stably transfected RAW 264.7 clones expressing wild-type (WT) or mutants of PAMM (C85G, C88G, C85G–C88G) were incubated for 5 days on 48-well plates in the presence of RANKL (50 ng/ml) and then stained for *TRAP*. Cells stably transfected with an empty vector (V) and mock-transfected cells (−) were used as controls. Cells expressing C85G, C88G, and C85G–C88G mutants generated numerous osteoclasts in response to RANKL, similar to mock-transfected cells or cells transfected with an empty vector. Cells transfected with a wild-type PAMM, conversely, did not form osteoclasts. (**A**, *bottom panel*) Western blot analysis of protein extracts from: mock-transfected RAW264.7 cells (−), wild-type PAMM (WT), C85G PAMM (85), C88G PAMM (88), C85G–C88G PAMM (85/88), and empty vector (V) by using an anti-PAMM and β-actin antibody shows that all transfected cells overexpress PAMM (with the exception of mock-transfected cells or cells transfected with an empty vector). (**B**) *TRAP* staining of: control RAW 264.7 cells (V), PAMM 1 and PAMM 2 stimulated with RANKL for 5 days without (−, *left column*) or with 50 μm H_2O_2 (+, *right column*) shows that the addition of H_2O_2 can reverse the effect of PAMM expression on osteoclast formation.

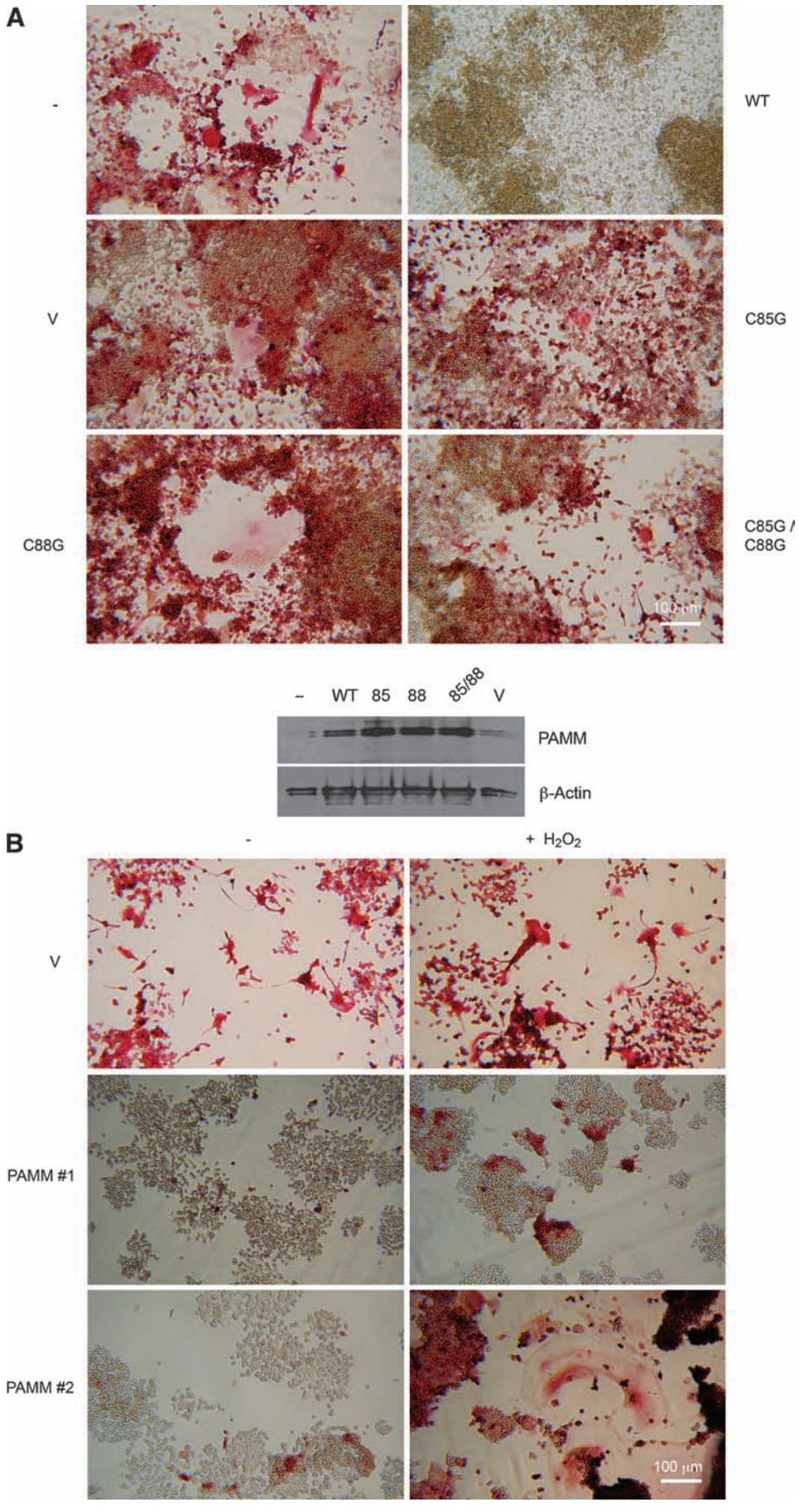
A
-
WT
V
C85G
C88G
C85G /
C88G
100 μm
- WT 85 88 85/88 V
PAMM
β-Actin
B
-
+ H2O2
V
PAMM #1
PAMM #2
100 μm

PAMM belongs to the (PRX)-like 2 family of proteins, which are related to peroxiredoxins by sequence similarity and also to thioredoxin, because they contain a CXXC motif, which is used by many enzymes in redox functions. The second cysteine of the CXXC motif corresponds to the peroxidatic cysteine of PRX and is presumed to be essential to alter the redox status of target proteins. This agrees with our observation that mutation of C88 (the second cysteine of the CXXC motif) has a larger effect in both PAMM redox activity and the inhibition of osteoclastogenesis. Because PAMM expression abolishes RANKL-induced NF-κB and Jun activation, these findings show that PAMM is involved in the regulation of redox status during osteoclast differentiation, and they suggest a new mechanism for ROS regulation of osteoclast activity and function.

PAMM was originally identified as a gene upregulated in osteoclasts by stimulation with both M-CSF and RANKL. We found that M-CSF alone was able to induce PAMM expression in monocytes. The addition of both M-CSF and RANKL resulted in slightly decreased PAMM expression in cell culture. This observation suggested that PAMM expression could play a dual role in osteoclastogenesis: inhibiting osteoclast differentiation while stimulating proliferation of osteoclast precursors by regulating the levels of intracellular ROS. RANKL induces the production of ROS that play a central role in osteoclastogenesis through the RANKL-TRAF6 axis (10). In addition, osteoclast formation is stimulated by hydrogen peroxide and inhibited by antioxidants such as *N*-acetyl cysteine (NAC), further demonstrating a role for ROS in osteoclast differentiation (22, 23).

Antioxidants regulate bone mass *in vivo* as well. For instance, although the mechanisms through which estrogen prevents bone loss are not fully elucidated, it is known that ovariectomy causes oxidative stress in bone. Consequently, levels of the main tissue thiol antioxidants, glutathione and thioredoxin, are substantially reduced in ovariectomized mice (23). Moreover, ovariectomy also caused a decrease in the level of the enzymes that regenerate the reduced forms of glutathione and thioredoxin in the bone marrow. Conversely, levels of both antioxidants as well as their regenerative enzymes, were rapidly normalized by a single injection of 17-β estradiol (11, 12). Finally, treatment with antioxidants prevented estrogen-deficiency bone loss, whereas drugs that result in reduced thiol antioxidant, like BSO, induced bone loss. Because we showed that PAMM expression in osteoclast precursors could inhibit osteoclast formation *in vitro,* it is possible that PAMM is a mediator of estrogen-induced inhibition of osteoclastogenesis. This view would establish a novel mechanistic link between ROS and enhanced bone resorption in which estrogen could protect bone by maintaining levels of proteins like PAMM. Estrogen deficiency, conversely, would result in lower expression of PAMM, leading to increased osteoclast formation and bone resorption. Further experiments aimed at determining the effect of estrogen on PAMM expression are currently under way.

Alternatively, PAMM expression could be induced by oxidative stress, as with other detoxifying enzymes (26, 29). Oxidative stress occurs when the normal balance between reactive oxygen species (ROS) and antioxidants is disrupted as the result of adverse physiological conditions. This may stem from a depletion of antioxidants or an excess accumulation of ROS, which overwhelms the natural coping defenses of the biologic system. Cells respond to oxidative stress by resetting critical homeostatic parameters to counteract the oxidant effects and to restore redox balance. One such cellular response involves the activation of oxidative stress–activated transcription factors (like NF-$\kappa\beta$ and Nrf2), leading to the expression of genes encoding antioxidant enzymes, like PAMM. In this view, PAMM expression would increase in bone marrow cells from ovariectomized animals, because oxidative stress that results from estrogen deficiency would trigger that homeostatic response. Further experiments, aimed at studying changes in the expression of PAMM as well as in the activation of NF-$\kappa\beta$ and Nrf2 in ovariectomized mice, also are under way.

In conclusion, we report the identification, expression, and functional analysis of a gene, *pamm*, which codes for a novel PRX-like 2 protein with redox regulatory activity. Expression of PAMM is increased in $CD14^+$ monocytes stimulated with M-CSF and decreases as M-CSF–stimulated cells undergo RANKL-dependent osteoclast differentiation. We have shown that overexpression of PAMM in RAW 264.7 cells is associated with inhibited NF-κB2 and AP-1 activation and impaired osteoclastogenesis in response to RANKL. We also have shown that cysteine residues at position 85 and especially cysteine at position 88 are required for those activities. Studies addressing the transcriptional control of PAMM expression by Nrf-2 and the expression of PAMM in bone *in vivo* after ovariectomy are currently under way. Understanding this novel mechanism will aid in the design of novel therapies to reduce oxidative stress by modulating PAMM expression or activity and potentially to prevent osteoporosis and other forms of bone loss.

Acknowledgments

We thank Ms Justine Dobeck for technical assistance and Subbiah Yoganathan for expertise with animal experimentation. The work was supported by grant K12 HD001097-08 to LRM from NIH/NICHD, and grant RO1 DE07444 to PRO from the US NIDCR. Opinions expressed are those of the authors and do not necessarily represent those of the US NIH.

Author Disclosure Statement

The authors have nothing to disclose.

References

1. Aitken CJ, Hodge JM, Nishinaka Y, Vaughan T, Yodoi J, Day CJ, Morrison NA, and Nicholson GC. Regulation of human osteoclast differentiation by thioredoxin binding protein-2 and redox-sensitive signaling. *J Bone Miner Res* 19: 2057–2064, 2004.
2. Almeida M, Han L, Martin-Millan M, Plotkin LI, Stewart SA, Roberson PK, Kousteni S, O'Brien CA, Bellido T, Parfitt AM, Weinstein RS, Jilka RL, and Manolagas SC. Skeletal involution by age-associated oxidative stress and its acceleration by loss of sex steroids. *J Biol Chem* 282: 27285–27297, 2007.
3. Asagiri M and Takayanagi H. The molecular understanding of osteoclast differentiation. *Bone* 40: 251–264, 2007.
4. Banfi G, Iorio EL, and Corsi MM. Minireview: oxidative stress, free radicals and bone remodeling. *Clin Chem Lab Med* 46: 1550–1555, 2008.

5. Banfi G, Malavazos A, Iorio E, Dolci A, Doneda L, Verna R, and Corsi MM. Plasma oxidative stress biomarkers, nitric oxide and heat shock protein 70 in trained elite soccer players. *Eur J Appl Physiol* 96: 483–486, 2006.
6. Basu S, Michaelsson K, Olofsson H, Johansson S, and Melhus H. Association between oxidative stress and bone mineral density. *Biochem Biophys Res Commun* 288: 275–279, 2001.
7. Battaglino R, Fu J, Spate U, Ersoy U, Joe M, Sedaghat L, and Stashenko P. Serotonin regulates osteoclast differentiation through its transporter. *J Bone Miner Res* 19: 1420–1431, 2004.
8. Battaglino RA, Pham L, Morse LR, Vokes M, Sharma A, Odgren PR, Yang M, Sasaki H, and Stashenko P. NHA-oc/NHA2: a mitochondrial cation-proton antiporter selectively expressed in osteoclasts. *Bone* 42: 180–192, 2008.
9. Boyce BF, Yamashita T, Yao Z, Zhang Q, Li F, and Xing L. Roles for NF-kappaB and c-Fos in osteoclasts. *J Bone Miner Metab* 23(suppl): 11–15, 2005.
10. Boyle WJ, Simonet WS, and Lacey DL. Osteoclast differentiation and activation. *Nature* 423: 337–342, 2003.
11. Chow JW. Ovariectomy and estrogen replacement in rodents. *Methods Mol Med* 80: 361–365, 2003.
12. Chow JW, Tobias JH, Colston KW, and Chambers TJ. Estrogen maintains trabecular bone volume in rats not only by suppression of bone resorption but also by stimulation of bone formation. *J Clin Invest* 89: 74–78, 1992.
13. Davies KJ. Oxidative stress: the paradox of aerobic life. *Biochem Soc Symp* 61: 1–31, 1995.
14. Droge W. Free radicals in the physiological control of cell function. *Physiol Rev* 82: 47–95, 2002.
15. Franco R, Schoneveld OJ, Pappa A, and Panayiotidis MI. The central role of glutathione in the pathophysiology of human diseases. *Arch Physiol Biochem* 113: 234–258, 2007.
16. Haddad JJ. Antioxidant and prooxidant mechanisms in the regulation of redox(y)-sensitive transcription factors. *Cell Signal* 14: 879–897, 2002.
17. Holmgren A. Antioxidant function of thioredoxin and glutaredoxin systems. *Antioxid Redox Signal* 2: 811–820, 2000.
18. Huh YJ, Kim JM, Kim H, Song H, So H, Lee SY, Kwon SB, Kim HJ, Kim HH, Lee SH, Choi Y, Chung SC, Jeong DW, and Min BM. Regulation of osteoclast differentiation by the redox-dependent modulation of nuclear import of transcription factors. *Cell Death Differ* 13: 1138–1146, 2006.
19. Kaptoge S, Welch A, McTaggart A, Mulligan A, Dalzell N, Day NE, Bingham S, Khaw KT, and Reeve J. Effects of dietary nutrients and food groups on bone loss from the proximal femur in men and women in the 7th and 8th decades of age. *Osteoporos Int* 14: 418–428, 2003.
20. Kikuyama A, Fukuda K, Mori S, Okada M, Yamaguchi H, and Hamanishi C. Hydrogen peroxide induces apoptosis of osteocytes: involvement of calcium ion and caspase activity. *Calcif Tissue Int* 71: 243–248, 2002.
21. Kim H, Kim IY, Lee SY, and Jeong D. Bimodal actions of reactive oxygen species in the differentiation and bone-resorbing functions of osteoclasts. *FEBS Lett* 580: 5661–5665, 2006.
22. Lean JM, Davies JT, Fuller K, Jagger CJ, Kirstein B, Partington GA, Urry ZL, and Chambers TJ. A crucial role for thiol antioxidants in estrogen-deficiency bone loss. *J Clin Invest* 112: 915–923, 2003.
23. Lean JM, Jagger CJ, Kirstein B, Fuller K, and Chambers TJ. Hydrogen peroxide is essential for estrogen-deficiency bone loss and osteoclast formation. *Endocrinology* 146: 728–735, 2005.
24. Maggio D, Barabani M, Pierandrei M, Polidori MC, Catani M, Mecocci P, Senin U, Pacifici R, and Cherubini A. Marked decrease in plasma antioxidants in aged osteoporotic women: results of a cross-sectional study. *J Clin Endocrinol Metab* 88: 1523–1527, 2003.
25. Morton DJ, Barrett-Connor EL, and Schneider DL. Vitamin C supplement use and bone mineral density in postmenopausal women. *J Bone Miner Res* 16: 135–140, 2001.
26. Niture SK, Kaspar JW, Shen J, and Jaiswal AK. Nrf2 signaling and cell survival. *Toxicol Appl Pharmacol* 2009 June 16 [Epub ahead of print].
27. Okamatsu Y, Kim D, Battaglino R, Sasaki H, Spate U, and Stashenko P. *MIP-1* gamma promotes receptor-activator-of-NF-kappa-B-ligand-induced osteoclast formation and survival 1. *J Immunol* 173: 2084–2090, 2004.
28. Pham L, Purcell P, Morse L, Stashenko P, and Battaglino RA. Expression analysis of nha-oc/NHA2: a novel gene selectively expressed in osteoclasts. *Gene Expr Patterns* 7: 846–851, 2007.
29. Scandalios JG. Oxidative stress: molecular perception and transduction of signals triggering antioxidant gene defenses. *Braz J Med Biol Res* 38: 995–1014, 2005.
30. Tang D, Shi Y, Kang R, Li T, Xiao W, Wang H, and Xiao X. Hydrogen peroxide stimulates macrophages and monocytes to actively release HMGB1. *J Leukoc Biol* 81: 741–747, 2007.
31. Van WL, Odgren PR, MacKay CA, D'Angelo M, Safadi FF, Popoff SN, Van HW, and Marks SC Jr. The osteopetrotic mutation toothless (tl) is a loss-of-function frameshift mutation in the rat Csf1 gene: evidence of a crucial role for CSF-1 in osteoclastogenesis and endochondral ossification. *Proc Natl Acad Sci U S A* 99: 14303–14308, 2002.
32. Yang M, Mailhot G, MacKay CA, Mason-Savas A, Aubin J, and Odgren PR. Chemokine and chemokine receptor expression during colony stimulating factor-1-induced osteoclast differentiation in the toothless osteopetrotic rat: a key role for CCL9 (*MIP-1*gamma) in osteoclastogenesis in vivo and in vitro. *Blood* 107: 2262–2270, 2006.

Address correspondence to:
Ricardo A. Battaglino, Ph.D.
140 The Fenway
Boston, MA 02115

E-mail: rbattaglino@forsyth.org

Date of first submission to ARS Central, September 9, 2009; date of final revised submission, November 23, 2009; date of acceptance, December 1, 2009.

Abbreviations Used

BM = bone marrow
BMM = bone marrow monocyte
BSO = buthionine sulfoximine
C10orf58 = chromosome 10 open reading frame 58
CSF-1 = colony-stimulating factor 1
GSH = reduced glutathione
GSSG = oxidized glutathione
M-CSF = macrophage colony-stimulating factor
PAMM = peroxiredoxin activated in M-CSF–activated monocytes
PBMC = peripheral blood mononuclear cell
RANKL = receptor activator for nuclear factor-κB ligand
ROS = reactive oxygen species
Tb = trabecular bone